

Low energy spin wave excitations in bilayered magnetic manganite $\text{La}_{2-2x}\text{Sr}_{1+2x}\text{Mn}_2\text{O}_7$ ($0.30 \leq x \leq 0.50$)

H. Martinho* and C. Rettori
*Instituto de Física "Gleb Wataghin", UNICAMP,
13083-970, Campinas, SP, Brazil.*

D. L. Huber
*University of Wisconsin, Dept. Phys.,
Madison, Wisconsin, 53706, USA.*

J. F. Mitchell
Materials Science Division, Argonne National Lab., Argonne, Illinois, 60439, USA

S. B. Oseroff
*San Diego State University,
San Diego, California, 92182, USA.*

We have studied the low-temperature behavior of the magnetization and the specific heat of the bilayered perovskite system $\text{La}_{2-2x}\text{Sr}_{1+2x}\text{Mn}_2\text{O}_7$, for $0.30 \leq x \leq 0.50$. Our analysis reveals that below 30 K the temperature dependence of the magnetization of the ferromagnetic samples, $x = 0.30, 0.32$, and 0.36 , in a field of 1T can be interpreted in terms of the thermal excitations of a two-dimensional gas of ferromagnetic magnons. The specific heat in zero field for these samples as for the $x = 0.50$ antiferromagnetic one, is linear with temperature between the range of $1.8\text{K} \leq T \leq 10\text{K}$. This behavior can be also explained by the magnon gas model. By comparing specific heat measurements in zero field with those taken in a field of 9T we are able to extract the lattice and electronic contributions and determine the in-plane exchange interactions. That are found to be in reasonable agreement with the values inferred from the analysis of the magnetization data and also with the values reported by inelastic neutron scattering studies. In addition, we found that the electronic density of states obtained for the $x = 0.50$ sample is in agreement with previous band structure calculations.

PACS numbers: 75.47.De;75.30.Ds;75.30.Et;75.40.Cx

I. INTRODUCTION

Manganese oxides with perovskite structure have been subject of intense study in recent years. This is in large part motivated by two main factors: their potential technological application, related to the Colossal Magnetoresistance (CMR) effect displayed by many of these oxides, and the large variety of magnetic/electronic phenomena such as double-exchange, superexchange, Jahn-Teller effect, charge/orbital ordering related to the CMR.[1, 2]

A common way to represent the manganese perovskite oxides is through the Ruddlesden-Popper series $(\text{R,A})_{n+1}\text{Mn}_n\text{O}_{3n+1}$ (R = rare-earth; A = alkaline metal). The basic structure of the series consists of alternate stacking of rock-salt type block layers $(\text{R,A})_2\text{O}_2$ and $n\text{-MnO}_2$ sheets along the c -axis, where n represents the number of adjacent MnO_2 sheets, a quan-

tity closely related to the effective dimensionality of the system. So, the $n = \infty$ series represents the prototype three-dimensional (3D) CMR material $(\text{R,A})\text{MnO}_3$, the subject of many investigations lately; $n = 1$ corresponds to compounds such as La_2CuO_4 , the metal oxide that originates the high- T_C superconducting cuprates family; $n = 2$ represents the bilayered magnetic manganite system $(\text{R,A})_3\text{Mn}_2\text{O}_7$. [3] This last system shows two-dimensional (2D) magnetic and electronic properties associated with a very large magnetoresistance (MR) $\rho(0)/\rho(H) \sim 20,000\%$ at $T_C \sim 130\text{K}$ and $H = 7\text{T}$ for $\text{La}_{1.2}\text{Sr}_{1.8}\text{Mn}_2\text{O}_7$. [3] For comparison, in the 3D Sr-doped $\text{La}_{0.85}\text{Sr}_{0.15}\text{MnO}_3$ the MR reaches $\sim 110\%$ at $H = 15\text{T}$ around T_C . [4]

The structure of the $n = 2$ bilayer system is shown in figure 1. It consists of pairs of corner shared MnO_6 octahedron stacked along the c -axis and isolated by La(Sr) atoms. The dashed lines enclose the unit cell of the bilayer system. Also, indicated in the figure are the intra- MnO_2 plane, J_{\parallel} , inter- MnO_2 planes, J_{\perp} , and inter-bilayers, J' , exchange constants.

By changing x , the hole-doped bilayers

*Electronic address: hercules@ifi.unicamp.br;
URL: <http://www.ifi.unicamp.br/gpoms>

II. EXPERIMENTAL DETAILS

Single crystals of $\text{La}_{2-2x}\text{Sr}_{1+2x}\text{Mn}_2\text{O}_7$ for $0.30 \leq x \leq 0.50$ were melt grown in flowing 20% O_2 (balance Ar) in a floating zone optical image furnace (NEC SC-M15HD). Magnetization measurements have been taken in a *Quantum Design* *dc* SQUID MPMS-5T magnetometer. The specific heat was measured using the specific heat insert of a *Quantum Design* PPMS-9T measurement system.

III. EXPERIMENTAL RESULTS

Figure 2 shows the field-dependent *dc*-magnetization curves, M vs H , taken at 10K for $H \parallel ab$ and $H \parallel c$. The measurements in all samples were made by zero field cooling (ZFC) to 10K, then the field was increased to 5T and decreased again to zero. For $x = 0.30, 0.32$ and 0.36 we observed the usual non-linear FM behavior. The $x = 0.50$ sample displays a linear AFM behavior with a slight anisotropy between the *c*-axis and the *ab*-plane plus a small non-linear FM-like behavior at low fields ($H < 10\text{kOe}$).

From the M vs H curves we obtain the saturation magnetization, M_S , for the FM samples. Using this values it is possible to estimate the effective spin of the Mn ions, since $S_{eff} = M_S/2\mu_B$, and compare it with the theoretical expected one, S_{eff}^{theo} .

Considering that the theoretical valance of the manganese ion in the undoped compound $x = 0$, $\text{La}_2\text{SrMn}_2\text{O}_7$, is $3+$, and that their electronic configuration is $3d^4 4s^0$, their expected average effective spin is $S_{eff}^{theo}(x = 0) = 2$. Under hole-doping this value will be reduced by $x/2$, giving $S_{eff}^{theo}(x) = (4 - x)/2$. On Table I, we note that the agreement between S_{eff} and S_{eff}^{theo} is at best reasonable. That indicates that the average spin model does not provide a very good description of the saturation magnetization.

TABLE I: M_S , S_{eff} and S_{eff}^{theo} for the FM samples.

x	$M_S(\text{emu/g})$	S_{eff}	S_{eff}^{theo}
0.30	68.5	1.63	1.85
0.32	77.3	1.92	1.84
0.36	75.3	1.86	1.82

Figure 3 shows the temperature dependence of magnetization, M vs T curves, for the FM samples. All samples were field cooled from 300 to 1.8K in a 1T applied field. The curves show a FM transition at $T_C \sim 100 - 140\text{K}$, as reported previously,[2] with a slight anisotropy between $H \parallel c$ and $H \parallel ab$, which approaches zero for $x = 0.32$.

In the left scale of the figure 4 the M vs T curves for the AFM sample are shown. The sample was field cooled from 750 to 1.8K in a 1T applied field. As pointed out by Kubota *et al.*[6] when analyzing their magnetic neutron diffraction data, this sample presents two kinds of

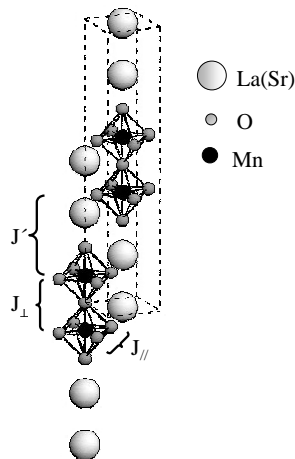


FIG. 1: Structure of the hole doped bilayered system $\text{La}_{2-2x}\text{Sr}_{1+2x}\text{Mn}_2\text{O}_7$. Dashed lines represents the unit cell of the bilayer where J_{\parallel} , J_{\perp} and J' are the exchange constants described in the text.

$\text{La}_{2-2x}\text{Sr}_{1+2x}\text{Mn}_2\text{O}_7$ present a wide variety of electron transport behaviour and magnetic structures. For the range $0.30 \leq x \leq 0.50$ it is found at low temperatures, $T < 10\text{K}$: (i) metallic character and ferromagnetic (FM) order along the *c*-axis for $x = 0.30$:[5] (ii) metallic character and FM order in the MnO_2 sheets (*ab*-plane) for $x = 0.32$; [5] (iii) metallic character and FM order in the *ab*-plane, with a weak antiferromagnetic (WAFM) component along the *c*-axis for $0.32 < x \leq 0.48$:[5] (iv) metallic A-type AFM with a small fraction ($< 18\%$) of a secondary CE-type AFM insulating phase for $0.48 < x \leq 0.50$.[6]

In all cases, the 2D character of the magnetic interactions is evident in these systems. For example, the measured critical exponent of the sublattice magnetization near T_C in the $x = 0.40$ sample,[7] was found to be very close to the expected value for the 2D Ising model.[8] The two-dimensionality of these systems is also revealed by the strong anisotropy in the resistivity, with the *ab*-plane resistivity being two or three orders of magnitude smaller than that along the *c*-axis.[3]

We have studied the influence of the dimensionality on the magnetization and specific heat of the $n = 2$ hole-doped bilayered system $\text{La}_{2-2x}\text{Sr}_{1+2x}\text{Mn}_2\text{O}_7$ ($0.30 \leq x \leq 0.50$). We present a consistent interpretation of the low-temperature data in terms of a gas of thermally excited 2D magnons.

AFM phases, an A-type and a CE-type. The Néel temperature of the A-AFM phase coincides with the charge ordering temperature at $T_{N,CO}^A = 210\text{K}$, while the CE-AFM orders at $T_N^{CE} = 145\text{K}$. [6] These two characteristic temperatures are shown in figure 4 by vertical dotted lines.

The right scale of figure 4 shows the temperature dependence of the inverse of magnetic susceptibility, χ^{-1} , for the $x = 0.50$ sample for both directions, $H \parallel c$ and $H \parallel ab$. Above $T \simeq 100\text{K}$ the two curves are identical. The number of effective Bohr magnetons, p_{eff} , and the Curie-Weiss temperature, θ , extracted from fitting the data to $\chi^{-1} = (T - \theta)/C$, for the range $600 < T < 750\text{K}$ are $p_{eff} = \sqrt{8C} = 4.59\mu_B/\text{Mn}$ and $\theta = 300\text{K}$. For this compound, the expected valance of Mn is 3.5 and $p_{eff} = 4.4\mu_B$, in good agreement with our experimental results.

Figure 5 shows the specific heat results plotted as C/T vs T^2 , at zero field and $H = 9\text{T}$, applied parallel to the c -axis for all samples. Two interesting features can be observed. The first one is the linear dependence of the zero-field data that shows a high value for gamma. This feature is basically independent of the hole concentration, magnetic order and conductivity. The second feature is the strong magnetic field dependence of the data. In the next section we will show that the origin of this behavior results from the 2D character of the system, namely, the influence of the 2D magnons. We will analyze the influence of the 2D magnons on the magnetization of the FM samples and on the specific heat of all compounds.

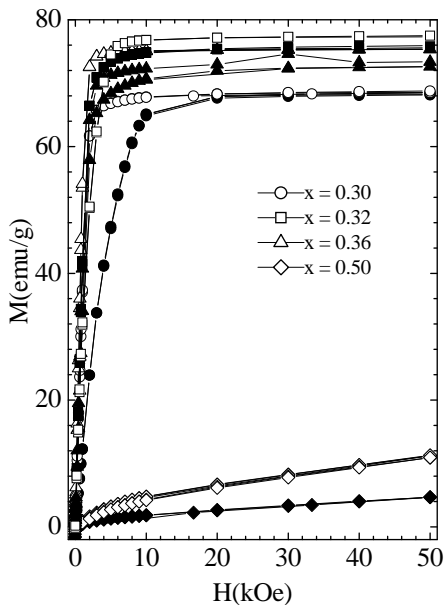


FIG. 2: M vs H measured at 10K for $x = 0.30, 0.32, 0.36$ and 0.50 samples. Solid symbols correspond to $H \parallel ab$ and open symbols to $H \parallel c$.

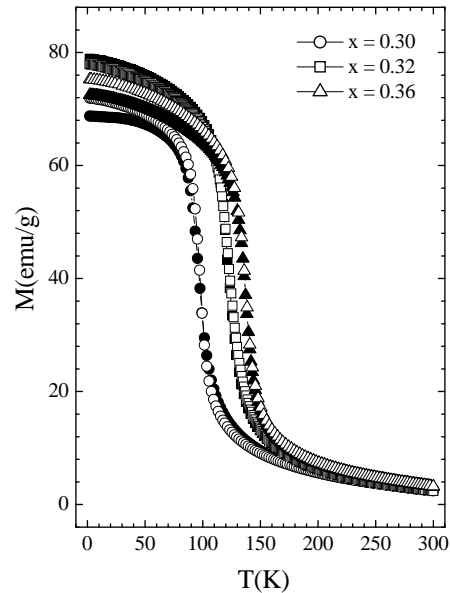


FIG. 3: M vs T for the FM samples $x = 0.30, 0.32$ and 0.36 taken at $H = 1\text{T}$. The solid symbols correspond to $H \parallel ab$ and open symbols to $H \parallel c$.

IV. THEORETICAL MODEL

A. Magnetization

To analyze the change on the magnetic response due to elementary excitations, it is useful to consider the fractional change of the magnetization, $[M(T \rightarrow 0) - M(T)]/M(T \rightarrow 0) \equiv \Delta M/M(0)$. Using boson statistics, it can be expressed as: [9]

$$\frac{\Delta M}{M(0)} = \frac{S - \langle S_z \rangle}{S} = \frac{1}{4\pi S} \int_0^\infty \frac{k dk}{e^{\frac{\hbar\omega(\mathbf{k})}{k_B T}} - 1}, \quad (1)$$

for spin waves in a system with both an acoustic and an optical branch, with the latter not thermally populated. Here S is the spin, $\langle S_z \rangle$ is the average value of the z component of the spin, \mathbf{k} is the magnon wave vector and $\hbar\omega(\mathbf{k})$ is the magnon energy.

Considering 2D FM acoustic magnons, with wave vector $\mathbf{k} = \mathbf{k}_a + \mathbf{k}_b$ (measured in units of the reciprocal of the nearest-neighbor distance, 3.87\AA), the dispersion relation at low temperatures, neglecting the interbilayer exchange energy J' , in the presence of a field, can be written as

$$\hbar\omega(\mathbf{k}) = -J_{\parallel} S \mathbf{k}^2 + 2\mu_B H = D \mathbf{k}^2 + \Delta, \quad (2)$$

with $D \equiv -J_{\parallel} S$ being the spin wave stiffness constant and $\Delta \equiv 2\mu_B H$ the gap induced by the magnetic field. Evaluating (1) using the dispersion relation (2), we obtain

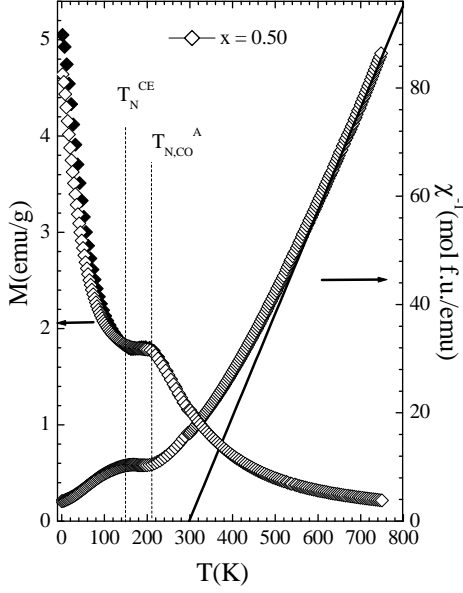


FIG. 4: *Left scale*: M vs T for the AFM sample $x = 0.50$ measured at $H = 1$ T. The vertical dotted lines represent the Néel temperatures of the two AFM phases at $T_N^{CE} = 145$ K for the CE type AFM structure and $T_{N,CO}^A = 210$ K for the A type one; *Right scale*: χ^{-1} vs T for the AFM sample $x = 0.50$, with the solid line showing the Curie-Weiss fitting for the parameters $p_{eff} = 4.59 \mu_B/\text{Mn}$ and $\theta = 300$ K. The solid symbols correspond to $H \parallel ab$ and the open symbols to $H \parallel c$.

$$\frac{\Delta M}{M(0)} = -\frac{T}{8\pi DS} \ln(1 - e^{-\frac{\Delta}{T}}), \quad (3)$$

with Δ in units of K.

The corresponding analysis for A-AFM magnons is more complicated and will not be discussed here.

B. Specific Heat

The contribution to the specific heat from the magnon excitations is calculated summing over harmonic oscillator-like contributions $\sim \left(\frac{\hbar\omega}{k_B T}\right)^2 \frac{e^{\frac{\hbar\omega}{k_B T}}}{(e^{\frac{\hbar\omega}{k_B T}} - 1)^2}$. We can express the total contribution to the specific heat coming from the acoustic branch of the 2D FM magnons having the dispersion relation (2) as

$$C_{mag} = \frac{1}{4\pi k_B T^2} \int_0^\infty \frac{k[\hbar\omega(k)]^2 e^{\frac{\hbar\omega(k)}{k_B T}}}{[e^{\frac{\hbar\omega(k)}{k_B T}} - 1]^2} dk \quad (4)$$

Using this expression we can derive the zero-field, $\Delta = 0$, 2D FM magnon specific heat as

$$C_{mag}(H = 0) = \frac{\pi R k_B}{24D} T \equiv \gamma_{mag} T, \quad (5)$$

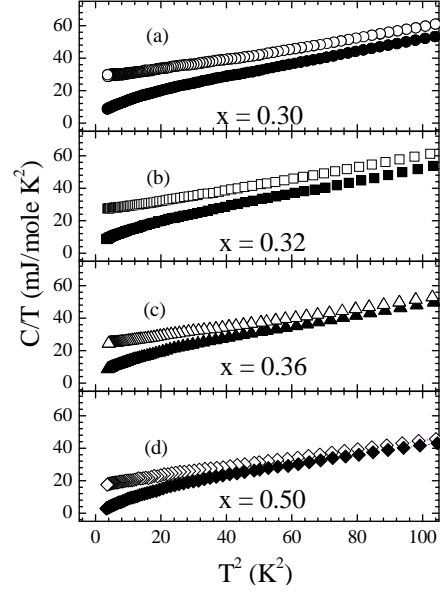


FIG. 5: C/T vs T^2 for $x = 0.30$ (a), 0.32 (b), 0.36 (c) and 0.50 (d) samples. Open symbols represent the zero field measurements. Solid symbols corresponds to measurements with $H = 9$ T $\parallel c$.

where $\gamma_{mag} = \pi R k_B / 24D$. This expression was first derived by Colpa[11] for a 2D Bravais lattice of spins. The field-dependent specific heat is obtained solving (4) with $\Delta \neq 0$. Unfortunately, in this case, the result is not analytical.

Neutron scattering results by Hirota *et al.*[12] indicate that the coupling between the two MnO_2 sheets, J_\perp , is nearly zero for $x = 0.50$. Thus, in the analysis of the specific heat for $x = 0.50$, we neglect J_\perp so that the magnetic contribution to the specific heat is the result of 2D excitations that are effectively FM for energies $\sim k_B T$. We can then use the expression (5) keeping in mind that in this case $\gamma_{mag} = \pi R k_B / 12D$, since there are two degenerate magnon branches for each k -value.

Considering the contributions to the specific heat coming from electrons, phonons, and magnons, the total zero-field specific heat can be described as

$$\frac{C}{T}(H = 0) = \gamma_e + \gamma_{mag} + \beta T^2 \equiv \gamma_{eff} + \beta T^2, \quad (6)$$

where we have defined an effective gamma-term $\gamma_{eff} = \gamma_e + \gamma_{mag}$. So, the zero field specific heat can be displayed as a linear plot in a C/T vs T^2 curve.

For $H \neq 0$ the total specific heat will be

$$\frac{C}{T}(H \neq 0) = \gamma_e + \beta T^2 + \frac{1}{4\pi k_B T^3} \int_0^\infty \frac{k[\hbar\omega(k)]^2 e^{\frac{\hbar\omega(k)}{k_B T}}}{[e^{\frac{\hbar\omega(k)}{k_B T}} - 1]^2} dk \quad (7)$$

with $\hbar\omega(k) = Dk^2 + \Delta$.

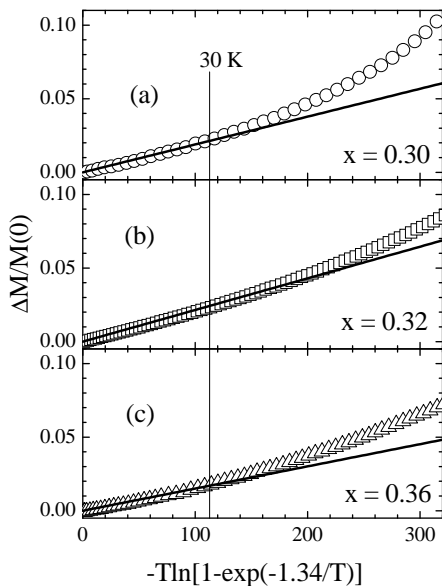


FIG. 6: $\Delta M/M(0)$ plotted as function of $-T \ln[1 - e^{-\frac{\Delta}{T}}]$ for $x = 0.30$ (a), 0.32 (b), and 0.36 (c). The magnetic field of $H = 1\text{T}$ ($\Delta = 1.34\text{K}$) was applied along the easy-axis. The vertical dotted line indicates the temperature of 30K . The solid line represents the fitting of $\Delta M/M(0)$ to $-bT \ln[1 - e^{-\frac{\Delta}{T}}]$.

For $x = 0.50$, the prefactor in front of the integral in eq.(7) need to be multiplied by a factor of 2 to account for the two-fold degeneracy mentioned previously.

In the next section we will apply these results to the analysis of the magnetization and specific heat data.

V. ANALYSIS AND DISCUSSION

A. Magnetization

Figure 6 shows the fractional change of the magnetization $\Delta M/M(0)$ as function of $-T \ln[1 - e^{-\frac{\Delta}{T}}]$ for the FM samples. A field of $H = 1\text{T}$ ($\Delta = 1.34\text{K}$) was applied parallel to the easy-axis of the samples: $\parallel c$ for $x = 0.30$ and $\parallel ab$ for $x = 0.32$ and 0.36 . We fit the data to $\Delta M/M(0) = -bT \ln[1 - e^{-\frac{\Delta}{T}}]$ and the parameters obtained are given in Table II.

TABLE II: Parameters b , D and J_{\parallel} , obtained as described in the text.

x	$b(10^{-4}\text{K}^{-1})$	$D(\text{K})$	$J_{\parallel}(\text{K})$
0.30	1.9(1)	112(6)	-60(2)
0.32	2.1(1)	104(6)	-56(2)
0.36	1.6(1)	138(9)	-76(4)

From the expression (3) we have that $b = 1/8\pi DS$. In order to enable us a consistent comparison between our model and the neutron diffraction analysis from

literature,[12, 13, 14, 15] we use the average theoretical effective spin S_{eff}^{theo} , instead of the experimental value S_{eff} . Using S_{eff}^{theo} we obtained the stiffness constant, D , and the exchange energy J_{\parallel} given in Table II. No significant differences are found if S_{eff} is used instead. In that case the values of J_{\parallel} are: $-78(4)$, $-52(2)$ and $-74(4)\text{K}$, for $x = 0.30$, 0.32 and 0.36 , respectively. Our values of J_{\parallel} are in good agreement with the J_{\parallel} values obtained from neutron diffraction measurements[12, 13, 14, 15]. Thus, from our analysis we can conclude that the main contribution to the temperature dependence of the magnetization of the FM bilayer system comes from the 2D FM magnons.

B. Specific heat

Figure 7 shows the zero field specific heat data fit to eq.(6). In the temperature interval between $1.8\text{K} \leq T \leq 10\text{K}$, the data are in a good agreement with the FM magnon model. From this analysis we derived the γ_{eff} and β values for all concentrations.

TABLE III: Experimental specific heat parameters.

x	γ_{eff} (mJ/mole K^2)	γ_e (mJ/mole K^2)	β (mJ/mole K^4)	$D(H = 9\text{T})$ (K)
0.30	28(1)	7.0(2)	0.27(3)	88(4)
0.32	25(1)	7.0(3)	0.31(3)	96(2)
0.36	23(1)	7.0(2)	0.27(2)	98(6)
0.50	24(1)	4.0(8)	0.40(4)	196(16)

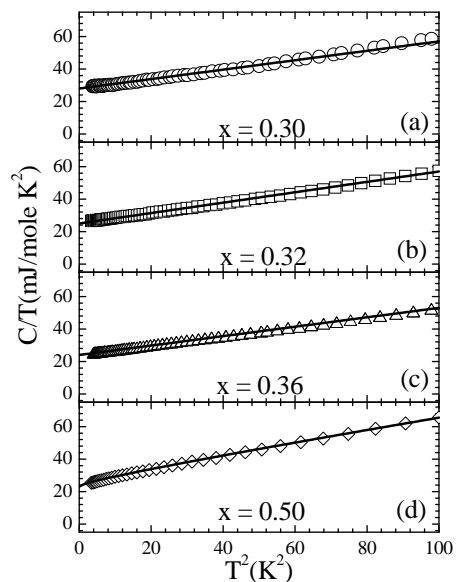


FIG. 7: Zero field specific heat data for $x = 0.30$ (a), 0.32 (b), 0.36 (c) and $x = 0.50$ (d) samples. The solid lines represents the fitting of the data to eq. (6).

TABLE IV: Parameters obtained from the specific heat analysis as described in the text.

x	$g(\varepsilon_F)$ (states/Ry f.u.)	γ_{mag} (mJ/mole K ²)	$D(H = 0)$ (K)	$J_{\parallel}(H = 0)$ (K)	$J_{\parallel}(H = 9T)$ (K)
0.30	40(1)	21(1)	104(2)	-56(2)	-47(1)
0.32	40(2)	18(1)	122(2)	-66(4)	-52(2)
0.36	40(1)	16(1)	136(2)	-74(4)	-54(2)
0.50	23(5)	20(1)	218(4)	-124(6)	-112(8)

Figure 8 shows the specific heat data, taken at $H = 9T$, fitted to eq.(7). In this fitting we used the β parameters derived from the zero field analysis. From it we obtain γ_e and $D(H = 9T)$ and calculated the exchange energy $J_{\parallel}(H = 9T)$. No appreciable difference is found in the J_{\parallel} values when using S_{eff}^{theo} or S_{eff} . For $x = 0.50$, it should be noted that the ferromagnetic approximation for the spin wave energies, as indicated by the linear behavior of the specific heat in zero field, only pertains to the modes that make a significant contribution in the temperature range of the experiment. If measurements were made at much lower temperatures, one would expect a temperature dependence characteristic of a weakly anisotropic A-AFM.

We calculated the γ_{mag} from $\gamma_{mag} = \gamma_{eff} - \gamma_e$. Using γ_e and γ_{mag} we computed the electron density of states at Fermi level, $g(\varepsilon_F)$, and $D(H = 0)$. Finally, from $D(H = 0)$ we obtain the exchange energy $J_{\parallel}(H = 0)$. The experimental parameters γ_{eff} , γ_e , β and $D(H = 9T)$ are listed in the Table III. The values of $g(\varepsilon_F)$, γ_{mag} , $D(H = 0)$, $J_{\parallel}(H = 0)$ and $J_{\parallel}(H = 9T)$ derived from the data, are given in the Table IV.

The values of γ_e and $g(\varepsilon_F)$ of the insulating samples, $x = 0.30, 0.32$ and 0.36 are in reasonable agreement with those reported in the literature (see, e.g., the results of Okuda *et al.*[16]), suggesting a half metallic behavior. In fact, electronic band structure calculations performed by Meskine *et al.*[17] suggested a half metallic character for some bilayers. In particular, for $x = 0.50$ they found the theoretical value of $g(\varepsilon_F) = 19$ states/Ry f.u., in excellent agreement with our experimental value of 23 states/Ry f.u..

The values of $J_{\parallel}(H = 0)$ and $J_{\parallel}(H = 9T)$ are in reasonable agreement with the results previously reported by neutron scattering studies[12, 13, 14, 15]. In figure 9 we compare the J_{\parallel} values obtained in the present work and the ones reported by Hirota *et al.*[12] The $J_{\parallel}(H = 0)$ values obtained from the zero field specific heat agree with the values inferred from the analysis of the magnetization. The values of $J_{\parallel}(H = 9T)$ differ somewhat from $J_{\parallel}(H = 0)$. That may be a consequence of the presence of the double exchange mechanism since J_{\parallel} is field-independent for a pure Heisenberg system. The $J_{\parallel}(H = 0)$ values are also in fair agreement with the Hirota's ones, while the $J_{\parallel}(H = 9T)$ are in excellent agreement. The above is possible related to the differences in the energy scale probed by the different techniques. Our zero field thermodynamic measurements probe lower en-

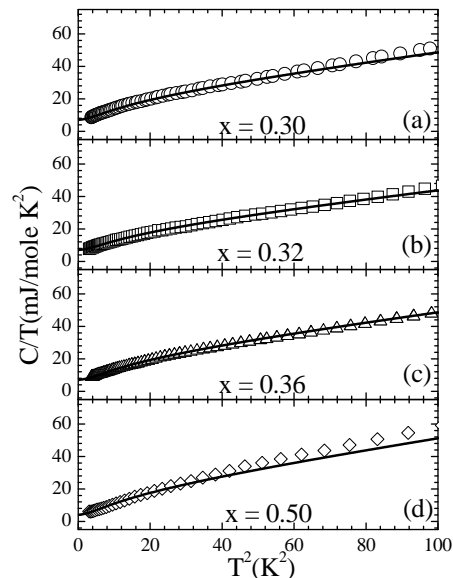


FIG. 8: Fit of the specific heat data measured at $H = 9T$ $\parallel c$ to eq.(7) for $x = 0.30$ (a), 0.32 (b), 0.36 (c), and 0.50 (d) samples.

ergy magnons, while the field-dependent measurements involve magnons with a slight higher energy, as the 9T magnetic field opens a gap ~ 1 meV in the magnon dispersion relation. On the other hand, generally neutron experiments involve magnons with energies $\gtrsim 3$ meV. So, it is expected a smaller difference between the values of J_{\parallel} derived from neutron diffraction and the obtained from 9T specific heat than with the ones extracted from the zero field specific heat. Also, a significant renormalization of the magnon energies at small k , that is not reflected in the neutron data, may be present.

VI. CONCLUSION

In summary, our experimental specific heat results reveal two interesting features: (i) the linear, high-gamma behavior of the zero-field data, independent of hole concentration, magnetic order or conductivity and (ii) the strong magnetic field dependence of the measurements.

We propose a model considering the presence of 2D FM magnons to explain the data. We calculated the influence of these magnons on the magnetization of the FM

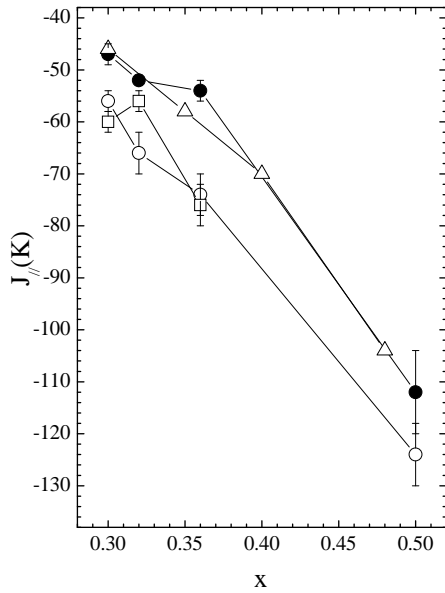


FIG. 9: Comparison between the J_{\parallel} values, obtained on the present work and the ones reported by Hirota *et al.*[12] Open squares correspond to the values derived from the $MvsT$ analysis. Open (solid) circles correspond to the values derived from $C/TvsT^2$ analysis with $H = 0(9T)$. Open triangles present the values from Hirota *et al.*[12]

samples and specific heat. In all the cases the model gives a good fit, showing that the change in magnetization and the specific heat of the system can be well described by a 2D FM magnon gas. In the case of the antiferromagnetic system ($x = 0.50$), the linear behavior of the specific heat is shown to be a consequence of the weak coupling between the bilayers sheets, that enables the occurrence of the 2D FM magnons.

As noted, we find similar values for J_{\parallel} from both the magnetization and the specific heat analysis, indicating an internal consistency on our analysis. Moreover, the values of J_{\parallel} we found are close to the ones derived from the neutron scattering studies[12, 13, 14, 15]. The last provides further support to our analysis.

VII. ACKNOWLEDGMENTS

This work was supported by the Brazilian Agencies CNPq and FAPESP and NSF 01-02235. D. L. Huber would like to thank T. G. Perring and N. Shannon for helpful comments.

-
- [1] see, e.g., D. M. Edwards, *Adv. Phys.* **51**, 1259 (2002); E. Dagotto, T. Hotta, and A. Moreo, *Phys. Reports* **344**, 1 (2001).
- [2] T. Kimura and Y. Tokura, *Annu. Rev. Mater. Sci.* **30**, 451 (2000).
- [3] Y. Moritomo, A. Asamitsu, H. Kuwahara, and Y. Tokura, *Nature* **380**, 141 (1996).
- [4] Urushibara, Y. Moritomo, T. Arima, A. Asamitsu, G. Kido, and Y. Tokura, *Phys. Rev. B* **51**, 14103 (1995).
- [5] M. Kubota, H. Fujioka, K. Hirota, K. Ohoyama, Y. Moritomo, H. Yoshizawa, and Y. Endoh, *J. Phys. Soc. Jpn.* **69**, 1606 (2000); M. Kubota, H. Fujioka, K. Hirota, K. Ohoyama, Y. Moritomo, H. Yoshizawa, and Y. Endoh, *J. Phys. Chem. Solids* **60**, 1161 (1999).
- [6] M. Kubota, H. Yoshizawa, and Y. Moritomo, *J. Phys. Soc. Jpn.* **68**, 2202 (1999).
- [7] R. Osborn, S. Rosenkranz, D. N. Argyriou, L. Vasiliu-Doloc, J. W. Lynn, S. K. Sinha, J. F. Mitchell, K. E. Gray, and S. D. Bader, *Phys. Rev. Lett.* **81**, 3964 (1998).
- [8] L. Onsager, *Phys. Rev.* **65**, 117 (1944).
- [9] O. Madelung, *Introduction to Solid-State Theory*, Springer-Verlag, Berlin (1996).
- [10] T. Oguchi, *Phys. Rev.* **117**, 117 (1960).
- [11] J. H. P. Colpa, *Physica* **57**, 347 (1972).
- [12] K. Hirota, S. Ishihara, H. Fujioka, M. Kubota, H. Yoshizawa, Y. Morimoto, Y. Endoh, and S. Maekawa, *Phys. Rev. B* **65**, 064414 (2002).
- [13] Tapan Chatterji, L. P. Regnault, P. Thalmeier, R. Suryanarayanan, G. Dhahlenne, and A. Revcolevschi, *Phys. Rev. B* **60**, 6965 (1999).
- [14] T. Chatterji, P. Thalmeier, G. J. McIntyre, R. van de Kamp, R. Suryanarayanan, G. Dhahlenne, and A. Revcolevschi, *Europhys. Lett.* **46**, 801 (1999).
- [15] T. G. Perring, D. T. Adroja, G. Chaboussant, G. Aeppli, T. Kimura, and Y. Tokura, *Phys. Rev. Lett.* **87**, 217201 (2001).
- [16] T. Okuda, T. Kimura, and Y. Tokura, *Phys. Rev. B*, **60**, 3370 (1999).
- [17] H. Meskine, Z. S. Popovic, and S. Satpathy, *Phys. Rev. B* **65**, 94402 (2000).